Journal of Engineering and Sustainable Development
Vol. 29, No. 05, A*ugust* 2025
https://jeasd.uomustansiriyah.edu.iq/index.php/jeasd
ISSN 2520-0917
Research Article
https://doi.org/10.31272/jeasd.3077

Ultra-Wideband Antenna Array for Modern Millimeter-Wave Wireless Applications

Hussam AL-Saedi[*1], Muhannad Y. Muhsin[2], Zainab F. Mohammad[1], Wael M. Abdel-Wahab[3]

[1]Communication Engineering Department, University of Technology, Baghdad, Iraq
[2]Electrical Engineering Department, University of Technology, Baghdad, Iraq
[3]Electrical and Computer Engineering, University of Waterloo, Canada

[*]Email: hussam.h.ali@uotechnology.edu.iq

Article Info

Received 29/10/2024
Revised 24/05/2025
Accepted 02/06/2025

Abstract

An ultra-wideband antenna with high gain performance for future 5G and beyond millimeter-wave (mm-wave) applications is presented in this paper. The proposed microstrip patch antenna element was designed based on an aperture-coupled microstrip patch with four loaded parasitic patches to improve the frequency bandwidth. The antenna was built by employing four metal layers. Roger RT/duroid 6006 and RT/duroid 6002 were used in this design as feeding and antenna substrates, respectively. The suggested antenna element was utilized to construct a 2×2 antenna array fed with a corporate feeding network to achieve high gain and desired radiation characteristics. ANSYSEDT 2022 R1 full-wave simulator was used to design and analyze the proposed antenna and the corporate feeding network. The array gain is between 9.5 dB and 13.2 dB over the desired band of interest. The attained reflection coefficient (S_{11}) of better than -10 dB is in the range of 26.15 GHz – 38.6 GHz, occupying a relatively compact antenna size. Moreover, the presented antenna realizes a low cross-polarization and a good front-to-back ratio. The obtained results show that the presented antenna can be considered an excellent candidate for modern wireless communication systems in mm-wave wideband applications.

Keywords: 5G and beyond communications, Array antenna, Loaded parasitic patches, Millimeter-wave applications, Ultra-wideband antenna.

1. Introduction

The development of wireless microwave components has surpassed that of the available communication systems over the past decade. By exploiting the present in-place network (3G network), 4G LTE technology has integrated a multitude of commercial services with high data rates, speed connectivity, and throughput. However, with the highly demanding intelligent services and new applications, this vast upgrading brings various challenges with the current available bandwidth that limit the requirement for an advanced wireless network. Thus, the new fifth generation is emerging [1],[2]. For 5G mobile communications, the 3 GPP (Third Generation Partnership Project) has introduced several fifth-generation bands, including low frequencies below 1 GHz, mid frequencies (sub-6 GHz), and millimeter-wave (mm-wave) frequencies above 24 GHz. The accessible spectrum within the mm-wave band is a great option to meet the requirements of the future 5G and beyond applications, given the limited supply of frequency spectrum below 6 GHz bands and the need for increased data rates.

Nevertheless, there are a few significant restrictions on this useful spectrum, including signal fading, atmospheric absorptions, and path loss attenuations. The aforementioned constraints are required to be overcome for wireless communication systems to operate more efficiently. In order to mitigate the limitations at mm-wave frequencies, an array made up of numerous antenna elements spaced optimally apart can produce a high gain, wide bandwidth, and respectable radiation pattern characteristics [3]-[6]. Accordingly, the design of a compact, simple, high-gain, wide-bandwidth, and high-radiation-efficiency antenna array is becoming a challenge to antenna designers.

A four-planar antenna array operating from 25.5 GHz to 29.5 GHz with a high gain of 10.2 dBi was presented in [7]. In [8], an antenna with a high gain of about 17 dBi was designed based on a multi-layered (four-layer) antenna element. A substrate integrated waveguide (SIW) based 4-element antenna array was introduced in [9]. Two dielectric resonators were located on an H-shaped slot etching from the top of the metal layer. In [10], a four-element antenna array based on a magneto-electric dipole antenna was exhibited. For gain and bandwidth enhancements, a meta-lens based on three split-ring resonators (SRRs) layers was employed. The antenna can work on a wideband range of frequencies, which is between 26.5 GHz and 38.3 GHz, with a high gain of 15 dBi. In [11], a four-element patch antenna array was suggested, where an electromagnetic bandgap (EBG) and dielectric superstrate were used for gain improvements. An ultra-wideband (UWB) multilayer antenna array design was presented in [12]. The bandwidth is in the range of 57 GHz to 71 GHz, and a gain of about 13.9 dBi was achieved. The design is based on an SIW configuration with several symmetric vias included. A four-element antenna array design based on a T-shaped antenna element was introduced in [13]. The antenna system operates within a bandwidth of 25.5 GHz to 30 GHz with a gain of 11.5 dBi. Although the antenna designs mentioned above have reasonable bandwidth and high gain, they are either complex structures or bulky configurations.

A simple, compact microstrip phased array antenna (PAA) was proposed in [14]. The antenna system operates at 28 GHz with a bandwidth of 1.7 GHz. In [15], a compact-sized antenna array design based on a multilayer coplanar waveguide was suggested. The proposed array operates at approximately 28 GHz with a 2 GHz bandwidth and has a gain of 11 dBi. In [16], a PAA system with 6 GHz bandwidth around 29 GHz and a gain of 13 dBi was offered. The antenna element was designed based on an open slot PIFA incorporated with the handset body. A PAA design based on two different antenna configurations was presented in [17]. The suggested four-element PAA system considered a quarter-wavelength notch and an aperture-coupled rectangular patch. Despite having compact sizes and relatively simple structures, the antenna designs mentioned above offer limited operating bandwidths. High data rate (gigabits per second (Gbps)) communication has only been possible with antenna systems owning a very large bandwidth. Furthermore, The ITU has offered numerous mm-wave bands for multi standard and various applications of communication systems, such as 26.5–29.5 GHz (Korea), 24.25– 27.5 GHz (EU), 26.5–27.5 GHz (Sweden), 27.5–28.35 GHz (USA), 25.3–27.5 GHz (China), 37–43.5 GHz (USA), and 27.5–28.28 GHz (Japan) [4]. So, a very wide bandwidth is inevitable for future communication systems. In addition, high-performance radiation characteristics of high gain with a simple structure and compact size in antenna system design have been strongly requested.

In this paper, an aperture-coupled rectangular microstrip patch antenna (ACRMPA) loaded with four parasitic rectangular microstrip patch antennas (PRMPAs) is introduced to realize an ultra-wideband antenna (UWBA) operating at mm-wave frequency band for modern 5G and beyond wireless communication systems. The proposed element was utilized to construct a 2×2 antenna array fed with a wideband, almost equal amplitude and phase microstrip corporate feeding network to enhance the overall antenna gain with uniform excitation to overcome the high path loss at millimeter frequencies. The suggested antenna array exhibited an impedance bandwidth with reflection coefficient (S_{11}) of better than -10 dB spanning the frequency range of 26.15 GHz – 38.6 GHz, occupying a relatively small footprint with an overall area of 10.2 mm × 10.2 mm, making it an excellent candidate for modern mm-wave wideband applications and phased array structures. Furthermore, it achieves a low cross-polarization level and a good front-to-back ratio.

2. Single Antenna Element Design

An aperture coupling-fed patch antenna loaded with parasitic patches is proposed and designed to realize a UWB operation. The configuration of the single antenna element and its layers are shown in Fig.1 (a) - Fig. 1 (f). The proposed antenna element was designed and optimized using ANSYSEDT 2022R1 full-wave simulator. It consists of four metal layers with three substrates. The two-aperture feeding metal layers, which are the bottom layers, are designed using Roger (RT/duriod 6006) substrate with an $\epsilon_r = 6.15$, loss tangent = 0.0019, and height of $h_1 = 0.127$ mm and $h_2 = 0.508$ mm, respectively. The size of the antenna substrate is $L_{sub} = 5.1mm$ and $W_{sub} = 5.1mm$. The aperture coupling antenna is fed by a 50 Ω microstrip feeding line with an open stub printed on the substrate and an aperture slot etched in the ground metal layer. The dimension of the microstrip feeding line is 2.54 mm, $Wf = 0.187\,mm$, while the open stub dimension is L_{stub} $0.46\,mm$. The dimensions of the aperture slot are $W_s = 0.261mm$ and $L_s = 1.847mm$. The rectangular patch primary antenna (third layer) is printed on the Roger (RT/duriod 6002) substrate with an $\epsilon_r = 2.94$, loss tangent = 0.0012, and height of $h_3 = 0.508mm$. The size of the rectangular patch antenna is $L_p = 1.92mm$ and $W_p = 2.2mm$, which is designed firstly according to the basic patch antenna in (1)-(4) to resonate at the center frequency of the operating bandwidth [18]-[22]. Width of the patch W_p is calculated:

$$\mathrm{W_p} = \frac{1}{2_{\mathrm{fr}}\sqrt{\mu_{0}\,\varepsilon_{0}}}\sqrt{\frac{2}{\varepsilon_{\mathrm{r}}+1}} \tag{1}$$

Length of the patch L_p:

$$\mathrm{L_p} = \frac{1}{{}_{2\mathrm{fr}}\sqrt{\varepsilon_{\mathrm{reff}}\quad \mu_{0}\,\varepsilon_{0}}} - 2\Delta\mathrm{L} \tag{2}$$

Effective relative permittivity ε_{reff}:

$$\varepsilon_{\mathrm{reff}} = \frac{\varepsilon_{\mathrm{r}}+1}{2} + \frac{\varepsilon_{\mathrm{r}}-1}{2}\left[1 + 12\ \frac{\mathrm{h}}{\mathrm{w_p}}\right]^{-\frac{1}{2}} \tag{3}$$

Extension of the length ΔL:

$$\Delta\mathrm{L} = 0.412\mathrm{h}\frac{(\varepsilon_{\mathrm{reff}\,+\,0.3})\left(\frac{\mathrm{W_p}}{\mathrm{h}} + 0.264\right)}{(\varepsilon_{\mathrm{reef}\,-\,0.258})\left(\frac{\mathrm{W_p}}{\mathrm{h}}\ + 0.8\right)} \tag{4}$$

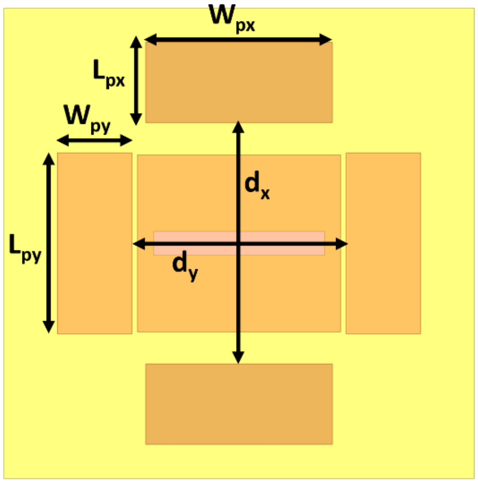

(a)

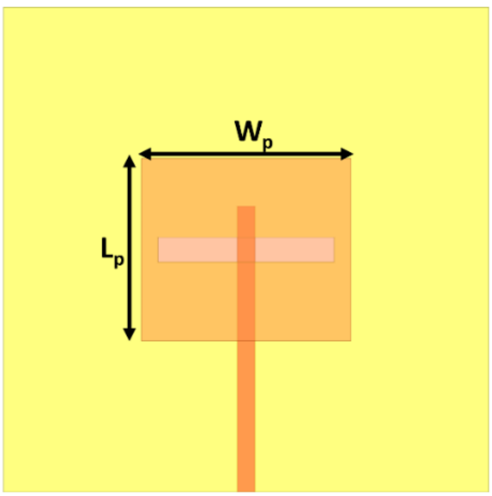

(b)

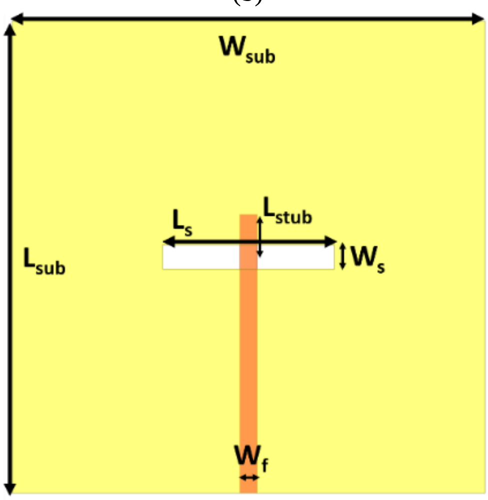

(c)

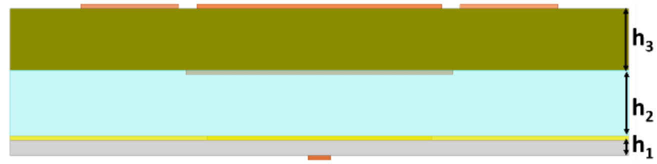

(d)

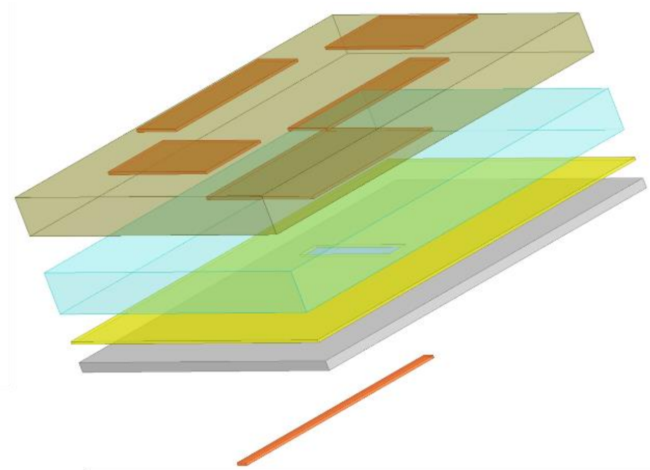

(f)

Figure 1. Proposed antenna element (a) parasitic patches, (b) primary antenna, (c) feed and aperture layers, (d) antenna cross section, and (f) antenna exploded view.

The fourth layer (upper layer) of the antenna element structure is loaded by four rectangular parasitic patches that enhance the impedance bandwidth; in addition to that, they improve the antenna gain effectively. These four rectangular parasitic patches are printed on the substrate, which has the exact specifications as the primary patch antenna substrate. The two patches located in the x-direction have the same size, which are $L_{px} = 0.875mm$ and $W_{px} = 2.02mm$. The distance between the x-patches $is\ dx = 2.6\ mm$. The other two parasitic patches placed in the y-direction have the same size, which are $W_{py} = 0.807mm$ and $L_{py} = 1.962mm$. The distance between these parasitic patches is $d_y = 2.32\ mm$.

The 50 Ω microstrip feed line is excited and coupled to the rectangular microstrip patch antenna through the coupling slot. For a typical narrow-band microstrip patch antenna, the patch size can be found using (1)-(4), the slot to operate as a coupling transformer, its length should be $L_s \approx 0.5\,\lambda_g$, and the stub length of the feed line should be in the range of $L_{stub} \approx 0.25\,\lambda_g$. On the other hand, making the antenna operate over a wide frequency range requires a significant modification of the typical antenna structure to provide multiple resonance modes that together can achieve an overall wideband operation. As a result, to realize such behavior, the patch antenna was loaded with parasitic patches with a superstrate as secondary radiators, resulting in a wide frequency band. A systematic design procedure is not found in literature due to the complexity of such a, problems, and researchers usually relyrely on full-wave simulators such as ANSYSANSYS, CST StudioStudio, and FEKO to tackle such difficulties.

The proposed antenna was simulated to evaluate its capabilities in terms of impedance bandwidth, gain, and radiation pattern. Fig. 2 demonstrates the simulated reflection coefficient where the proposed antenna achieved an $S_{11} < -10dB$ over the frequency range from 24.9 GHz to 39.25 GHz, realizing a fractional bandwidth of 44.7%. This significant bandwidth enhancement is attributed to the presence of the superstrate and parasitic patches that behave as additional resonators. This behavior can be observed by inspecting the S_{11} shown in Fig. 2, where at least two more resonance modes appeared at 34 GHz and 37 GHz, respectively.

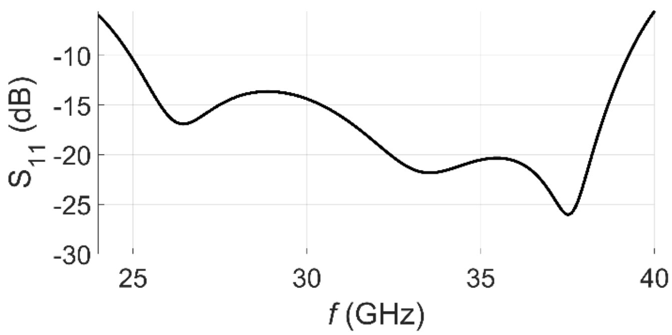

Figure 2. Simulated S_{11} of the proposed antenna.

The simulated gain is shown in Fig. 3, where the proposed antenna realized a maximum gain of 7.2 dB at 36.1 GHz with a gain variation of less than 0.6 dB over the operating bandwidth. The gain improvement can be related to the configuration of the proposed antenna, where the rectangular patch can be considered as the driven element. In contrast, the parasitic elements form an array excited by the main radiator. Hence, a proper choice of the superstrate thickness and the size and location of the parasitic patches plays a crucial role in achieving the best frequency band and gain.

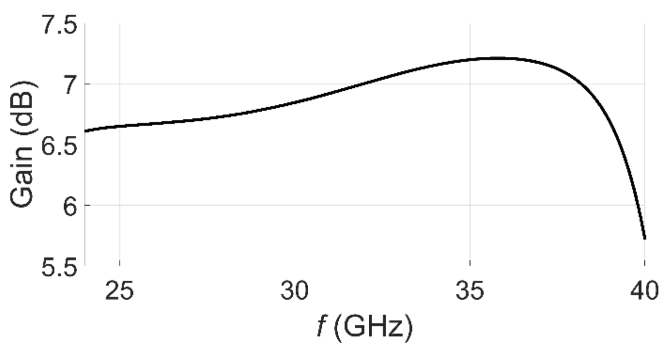

Figure 3. Simulated gain of the proposed antenna.

The radiation pattern of the antenna at two different frequencies, namely 28 GHz and 38 GHz, is illustrated in Fig. 4 at the E-plane and H-plane, where the proposed antenna attained an x-polarized pattern. It realizes a cross-polarization discrimination of 56.5 dB and front-to-back ratio (F/B) of 14.6 dB at 28 GHz in both E- and H-planes as depicted in Fig. 4(a) and Fig. 4(b), respectively. Moreover, the simulated radiation pattern at 38 GHz shows that the cross-polarization discrimination is better than 55 dB and F/B of 11.6 dB at 38 GHz in both E- and H-planes as depicted in Fig. 4(c) and Fig. 4(d), respectively. Aperture coupling excitation provides good isolation of spurious radiation and F/B ratio; furthermore, the size and distance of the x-directed and y-directed patches were optimized to minimize the cross-polarization level of the proposed antenna. As a result, the parameters L_{px}, W_{px}, and d_x differ from L_{py}, W_{py}, and d_y, respectively.

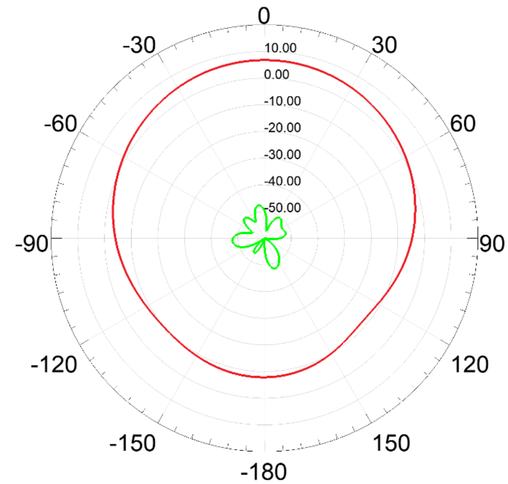

(a)

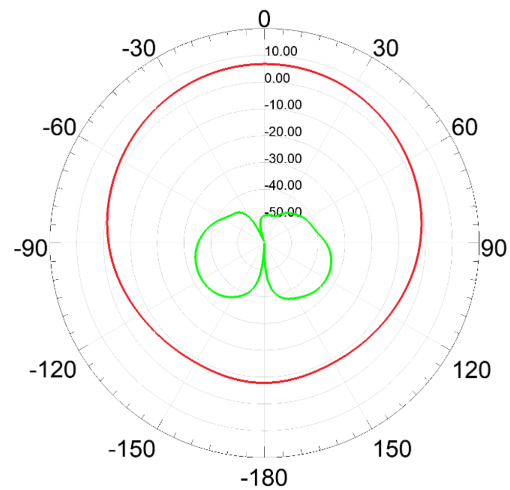

(b)

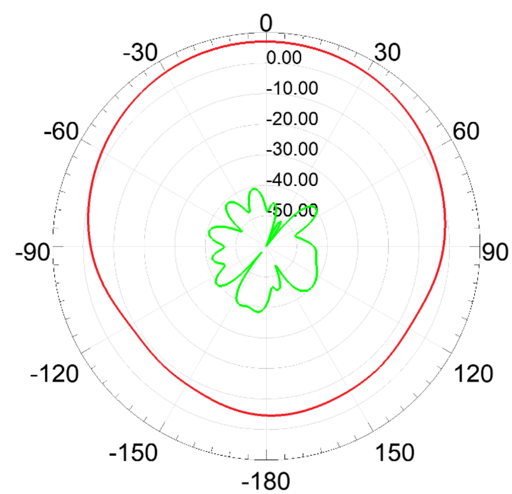

(c)

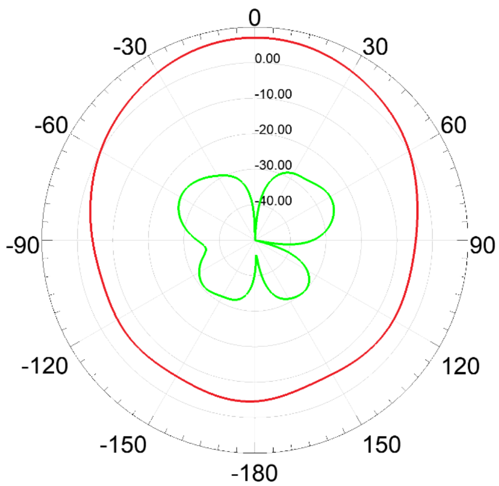

(d)

Figure 4. Simulated radiation pattern of the proposed antenna at (a) 28 GHz E-plane, (b) 28 GHz H-plane, (c) 38 GHz E-plane, and (d) 38 GHz H-plane.

3. Single Antenna Parameters Analysis

The antenna parameters were tested to study their impact on the impedance bandwidth to determine the optimal values. The slot length (L_s) was varied from 1.5 mm to 2.3 mm that resulted in significant variation of the S_{11} level especially at the lower frequencies where increasing L_s leads to shift the first resonance mode toward lower frequencies while the upper frequency stays almost unchanged as shown in Fig. 5. Accordingly, the operating bandwidth can be enhanced by proper choice of L_s while maintaining S_{11} below -10 dB.

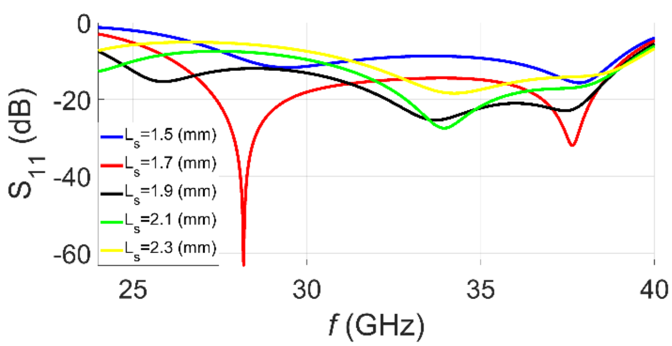

Figure 5. Impact of L_s on S_{11}.

The S_{11} level over the operating frequency band was affected as the stub length (L_{stub}) changed. Fig. 6 demonstrates the influence of L_{stub} on S_{11}; it can be noticed from this figure that as L_{stub} increases, the S_{11} level decreases at lower frequencies while it increases at higher frequencies and vice versa; hence, L_{stub} can be utilized to enhance the matching level within the operating band.

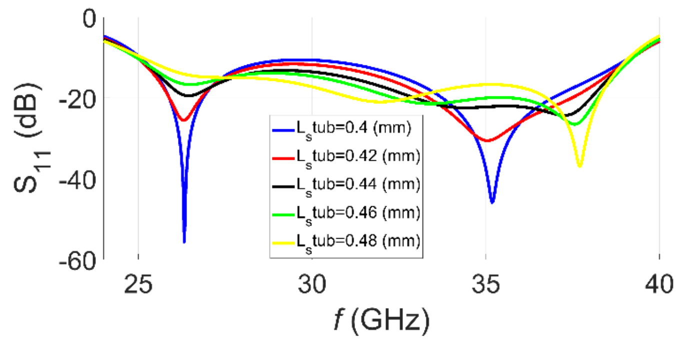

Figure 6. Impact of L_{stub} on S_{11}.

Fig. 7 depicts the impact of the L_{py} on the S_{11} of the proposed antenna. It mainly varies the impedance matching and the location of the resonance modes at upper frequencies, while at the lower frequencies, only the S_{11} level changes. As a result, L_{py} can be employed to control the upper limit of the operating frequency.

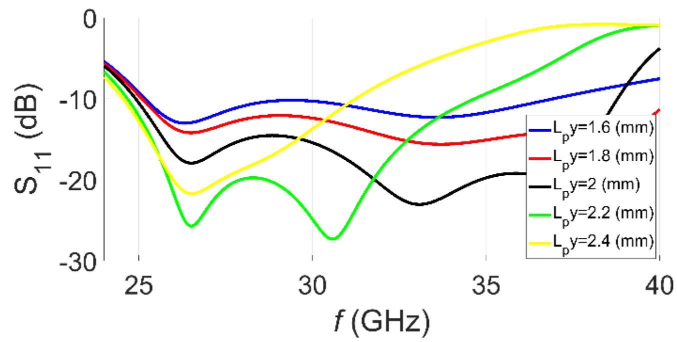

Figure 7. Impact of L_{py} on S_{11}.

Similarly, W_{py} was varied from 0.4 mm to 1.2 mm to study its influence on S_{11}, as depicted in Fig. 8, where increasing W_{py} improves the S_{11} level, but at the same time, the upper frequency limit is reduced significantly.

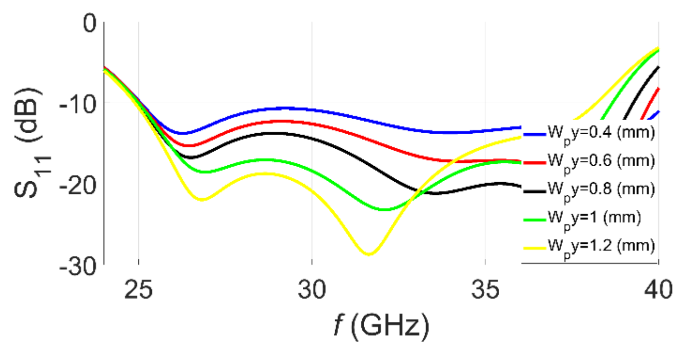

Figure 8. Impact of W_{py}on S_{11}.

4. Feeding Network

A UWB corporate feeding network based on one-to-four power division was proposed to distribute the power uniformly among the array elements. It splits the input power equally with the same amplitude and phase so that a bore-sight radiation can be realized over the operating bandwidth. The proposed feeding network was built to construct a 2×2 array as shown in Fig. 9. The feeding system and the distance between antennas were optimized to obtain the desired radiation properties. It consists of four main components, i.e., microstrip lines, 90^0 bends, power splitters, and $\lambda_g/4$ impedance transformers. A microstrip feed line with a characteristic impedance (Z_0) of 50 Ω was used to excite the antenna array, followed by a $\lambda_g/4$ impedance transformer, and a T-junction power splitter, which divides the input power equally with 3 dB power division and zero phase difference. The width of the T-junction lines was the same as the W_f, realizing a $Z_{in} = 25\ \Omega$ at the junction. In addition, the dimensions of the quarter wavelength were set to be $L_g \approx {}^{\lambda_g}/_4$ at the center frequency, and W_g was calculated to realize a $Z_{\lambda_g} = \sqrt{Z_{in} Z_{50\Omega}}$ matching the feeding line to the antenna impedance [23]. The dimensions of the $\lambda_g/4$ transformer were $L_g = 1.127mm \times W_g = 0.37mm$. The T-junction was then connected to two 50 Ω lines, where each was connected to a $\lambda_g/4$ line and a T-junction. Finally, four 50 Ω lines with 90^0 bends were employed to excite the array elements.

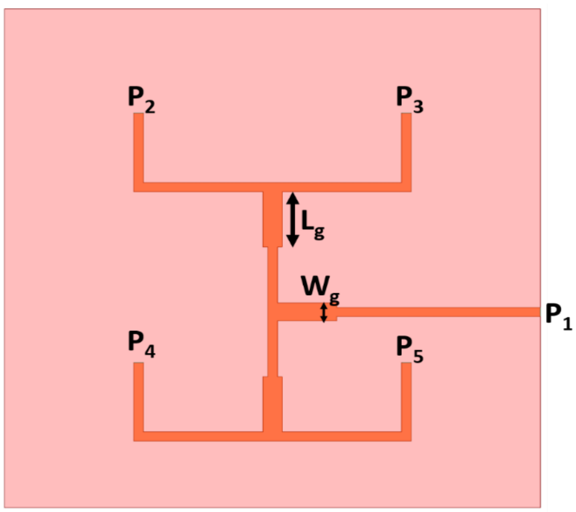

Figure 9. 1:4 Corporate feeding network.

The feeding network was simulated over the operating frequency band to validate the power distribution from the input port (P_1) to the output ports (P_i), where i≠= 1. Fig. 10 presents the S_{11} of the feeding network (P_1); it can be seen that S_{11} is almost below -10 dB over the frequency range from 25 GHz to 40 GHz, which suits the operation of the proposed antenna.

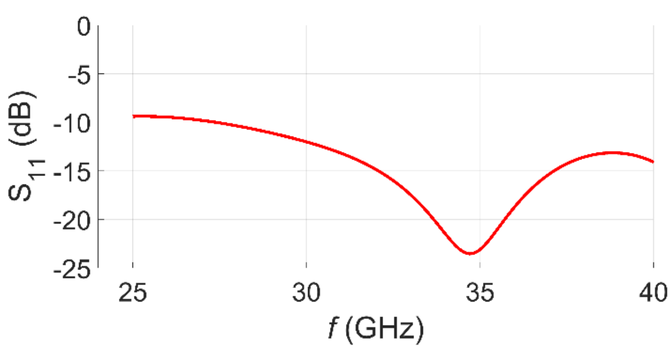

Figure 10. Simulated S_{11} of the feeding network.

By examining the amplitude and phase of the power transferred from the P_1 to P_i, it can guarantee uniform amplitude excitation to the antenna elements of the array with equi-phase distribution, generating maximum achievable directivity towards the boresight direction. Fig. 11 and Fig. 12 display the amplitude and phase distribution of the feeding network, respectively.

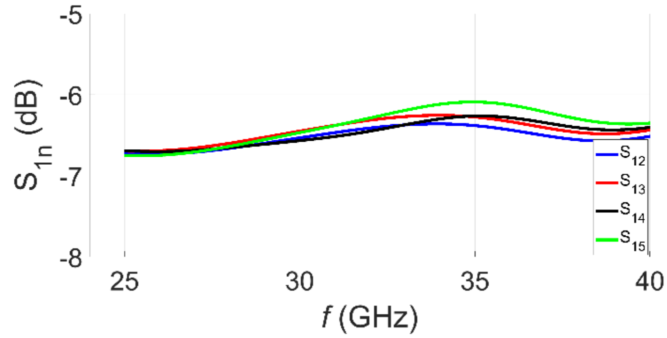

Figure 11. Simulated S_{1n} amplitude of the feeding network.

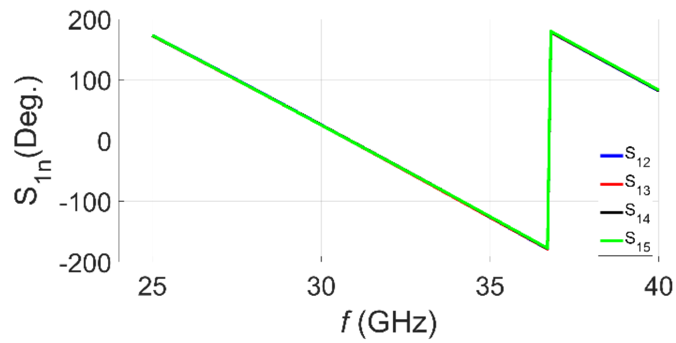

Figure 12. Simulated S_{1n} phase of the feeding network.

After designing the feeding network, four antenna elements and the feeding network were combined to realize a 2×2 array to achieve high gain and desired radiation characteristics for UWB mm-wave wireless communication applications, as shown in Fig.13. The overall dimensions of the antenna array system are (10.2 mm × 10.2 mm).

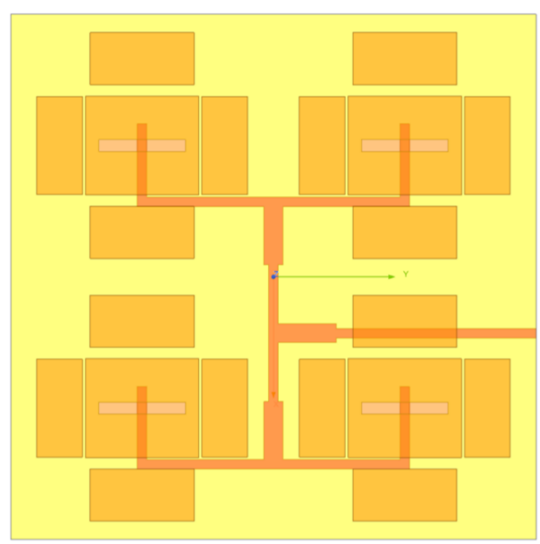
Figure 13. 2×2 Proposed antenna array.

The simulated reflection coefficient of the proposed 2×2 antenna array is shown in Fig. 14. UWB performance was obtained spanning the frequency range (26.15 GHz - 38.6 GHz), realizing a frequency bandwidth of 12.45 GHz. This high range of bandwidth is highly sought for high data rates and covers a wide range of mm-wave applications in future wireless communication systems. It is worth mentioning that the reduction of the operating band of the array compared with a single element is attributed to the presence of the feeding network, where the quarter-wave length transformer operates perfectly in the vicinity of the center frequency. As the frequency deviates, the transformer's performance deteriorates gradually. Moreover, the impact of the mutual coupling contributes to such bandwidth reduction.

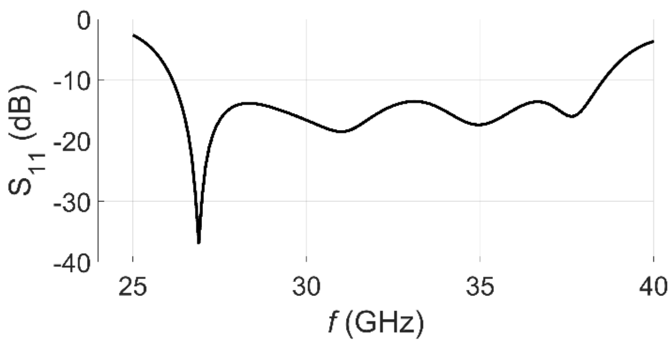

Figure 14. Simulated S_{11} of the 2×2 antenna array.

Fig. 15 presents the gain of the suggested antenna array system. High gain is achieved, which is between (9.5 dB and 13.2 dB). The maximum gain is 13.2 dB at 36.7 GHz, while the minimum gain is 9.5 dB at 26.6 GHz. As observed, high gain is attained to overcome the path losses in the mm-wave spectrum.

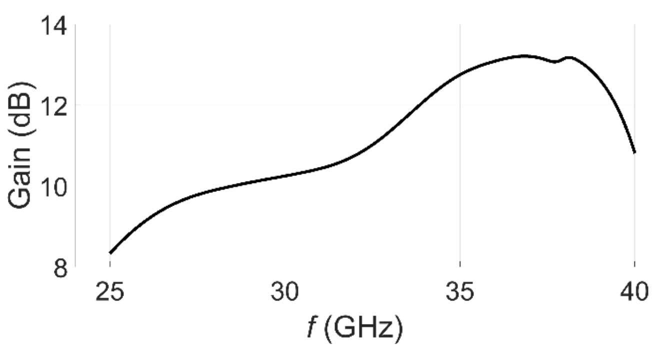

Figure 15. Simulated gain of the 2×2 antenna array.

The radiation pattern of the 2×2 antenna array at two different frequencies, namely 28 GHz and 38 GHz, is illustrated in Fig. 16(a)- Fig. 16(c) at E-plane and H-plane, where the proposed antenna attained an x-polarized pattern. It realizes a cross-polarization discrimination of 37.6 dB and front-to-back ratio (F/B) of 12.8 dB at 28 GHz in both E- and H-planes as depicted in Fig.16 (a) and Fig. 16(b), respectively. Moreover, the simulated radiation pattern at 38 GHz shows that the cross-polarization discrimination is better than 39 dB and F/B of 14.6 dB at 38 GHz in both E- and H-planes as depicted in Fig.16(c) and Fig.16(d), respectively.

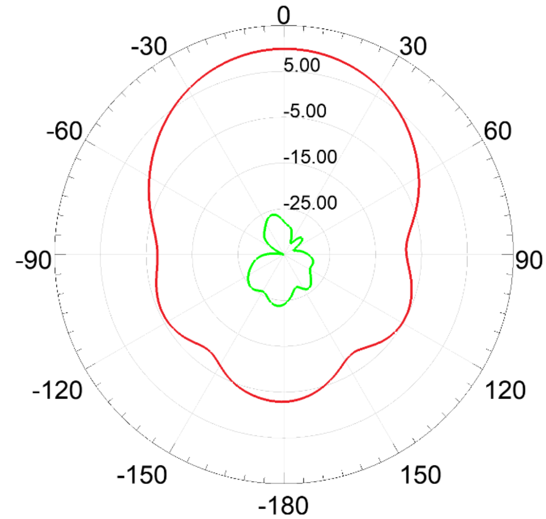

(a)

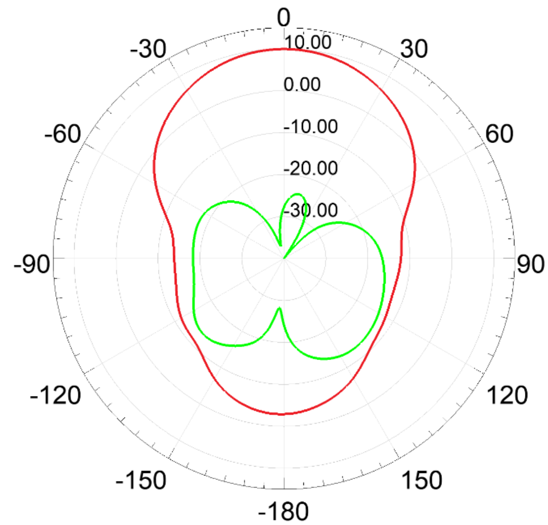

(b)

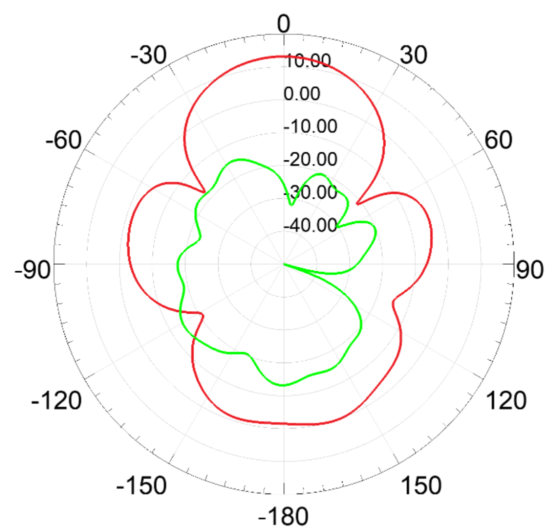

(c)

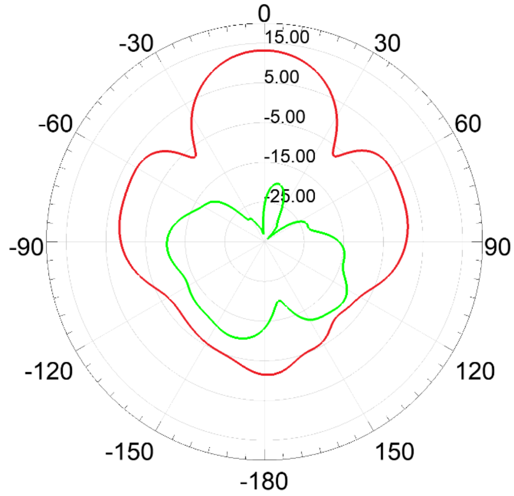

(d)

Figure 16. Simulated radiation pattern of the proposed 2×2 antenna array at (a) 28 GHz E-plane, (b) 28 GHz H-plane, (c) 38 GHz E-plane, and (d) 38 GHz H-plane.

The 3-D radiation pattern of the 2×2 antenna array at 28 GHz and 38 GHz is illustrated in Fig. 17.

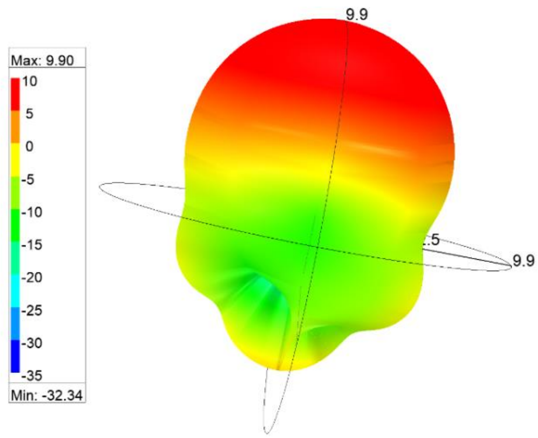

(a)

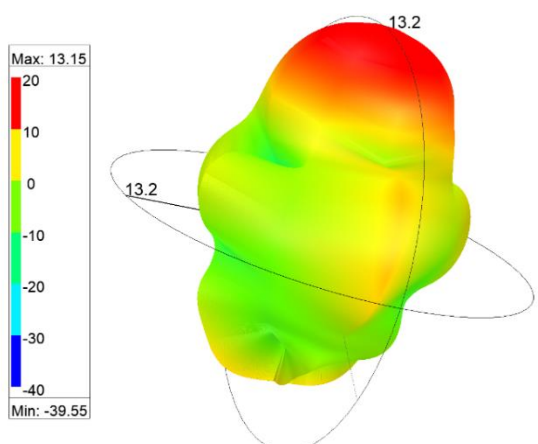

(b)

Figure 17. Simulated 3-D radiation pattern of the proposed 2×2 antenna array at (a) 28 GHz E-plane and (b) 28 GHz H-plane.

Table 1 compares the proposed antenna array with the relevant antenna arrays operating within a similar frequency band. It can be noticed that the suggested antenna surpasses the relevant antennas in terms of operating bandwidth, except references [5] and [6], where the presented antenna outperforms these antennas in terms of gain. Moreover, it shows a better gain level than four-element arrays. Accordingly, the proposed antenna is a good candidate for future applications in 5G mm-wave systems.

Table 1. Comparison of the proposed UWBA with the state-of-the-art.

Ref.	Operating frequency (GHz)	FBW (%)	No. of elements	Peak Gain (dBi)
[1]	23.41-33.92	36.7	4	10.7
[24]	26.3-30.7	15.5	4	8.71
[6]	24.35-31.13	24.4	16	19.9
[8]	26–45	53.5	4	12
[9]	26-38.5	38.7	4	11.5
This work	26.15 - 38.6	38.5	4	13.2

5. Conclusions

This paper introduced a new ultra-wideband antenna with high gain and desirable radiation characteristics for the upcoming 5G and beyond wireless communication systems. An aperture-coupled rectangular microstrip patch antenna loaded with four parasitic rectangular microstrip patch antennas was presented. The high coupling design between the aperture-coupled feeding and rectangular parasitic patches provides better impedance matching over UWB frequencies. The suggested antenna has a simple structure and compact size. To achieve high gain and anticipated radiation characteristics, the antenna element was applied to construct a 2×2 antenna array fed with a microstrip corporate feeding network. High gain was achieved, which is between (9.5 dB and 13.2 dB), to overcome the path losses in the mm-wave spectrum. The maximum gain is 13.2 dB at 36.7 GHz, while the minimum gain is 9.5 dB at 26.6 GHz. UWB performance was obtained spanning the frequency range (26.15 GHz - 38.6 GHz), realizing a frequency bandwidth of 12.45 GHz. This high bandwidth range is highly sought for high data rates and covers a wide range of mm-wave applications in future wireless communication systems. Based on the attained results, it can be concluded that the proposed antenna is a great option for future generation wireless communication systems in mm-wave applications. The proposed antenna and feeding network can be modified to meet the requirements for various modern wireless communication systems, to name a few: MIMO antenna for 5G and beyond, Ka-band satellite communications, and active phased array antenna.

Conflict of interest

The authors declare that there are no conflicts of interest regarding the publication of this manuscript.

Author Contribution Statement

Hussam Al-Saedi: proposed the concept, developed the antenna element and array configuration, and drafted the initial version of the manuscript.
Muhannad Y. Muhsin: executed the parametric analysis of the antenna element, array optimization, and contributed to the final draft of the manuscript.
Zainab F. Mohammad: designed the corporate feeding network and analyzed it, and also contributed to the initial draft of the manuscript.
Wael M. Abdel-Wahab: commanded the research tasks and contributed to the writing and reviewing of the final manuscript.

References

[1] [H. Ullah and F. A. Tahir, "A high gain and wideband narrow-beam antenna for 5G millimeter-wave applications," *IEEE Access*, vol. 8, pp. 29430–29434, 2020. https://doi.org/10.1109/ACCESS.2020.2970753.

[2] P. Ramanujam, C. Arumugam, R. Venkatesan, and M. Ponnusamy, "Design of compact patch antenna with enhanced gain and bandwidth for 5G mm-wave applications," *IET Microwaves, Antennas & Propagation*, vol. 14, no. 12, pp. 1455–1461, 2020. https://doi.org/10.1049/iet-map.2019.0891.

[3] M. Y. Muhsin, A. J. Salim, and J. K. Ali, "An eight-element multi-band MIMO antenna system for 5G mobile terminals," in *AIP Conference Proceedings*, vol. 2651, no. 1, 2023. https://doi.org/10.1063/5.0105773.

[4] M. Khalily, R. Tafazolli, P. Xiao, and A. A. Kishk, "Broadband mm-wave microstrip array antenna with improved radiation characteristics for different 5G applications," *IEEE Trans. Antennas Propag.*, vol. 66, no. 9, pp. 4641–4647, 2018. https://doi.org/10.1109/TAP.2018.2845451.

[5] I. Ahmad, H. Sun, U. Rafique, and Z. Yi, "Triangular slot-loaded wideband planar rectangular antenna array for millimeter-wave 5G applications," *Electronics*, vol. 10, no. 7, p. 778, 2021. https://doi.org/10.3390/electronics10070778.

[6] M. E. Munir et al., "A new mm-wave antenna array with wideband characteristics for next generation communication systems," *Electronics*, vol. 11, no. 10, p. 1560, 2022. https://doi.org/10.3390/electronics11101560.

[7] K. Raheel et al., "E-shaped H-slotted dual band mmWave antenna for 5G technology," *Electronics*, vol. 10, no. 9, pp. 1–10, 2021. https://doi.org/10.3390/electronics10091019.

[8] M. Sokol et al., "Design and simulation of ultra-wideband linearly tapered slot antenna for mm-wave applications," in *2023 24th International Radar Symposium (IRS)*, Berlin, Germany, 2023, pp. 1–7. https://doi.org/10.23919/IRS57608.2023.10172468.

[9] N. Ashraf, H. Vettikalladi, and M. A. Alkanhal, "A DR loaded substrate integrated waveguide antenna for 60 GHz high speed wireless communication systems," *Int. J. Antennas Propag.*, vol. 2014, no. 1, p. 146301, 2014. https://doi.org/10.1155/2014/146301.

[10] A. Dadgarpour, M. S. Sorkherizi, and A. A. Kishk, "Wideband low-loss magnetoelectric dipole antenna for 5G wireless network with gain enhancement using meta lens and gap waveguide technology feeding," *IEEE Trans. Antennas Propag.*, vol. 64, no. 12, pp. 5094–5101, 2016. https://doi.org/10.1109/TAP.2016.2620522.

[11] O. M. Haraz, A. Elboushi, S. A. Alshebeili, and A. R. Sebak, "Dense dielectric patch array antenna with improved radiation characteristics using EBG ground structure and dielectric superstrate for future 5G cellular networks," *IEEE Access*, vol. 2, pp. 909–913, 2014. https://doi.org/10.1109/ACCESS.2014.2352679.

[12] S. J. Park, D. H. Shin, and S. O. Park, "Low side-lobe substrate-integrated-waveguide antenna array using broadband unequal feeding network for millimeter-wave handset device," *IEEE Trans. Antennas Propag.*, vol. 64, no. 3, pp. 923–932, 2015. https://doi.org/10.1109/TAP.2015.2513075.

[13] S. H. Kiani et al., "Square-framed T shape mmWave antenna array at 28 GHz for future 5G devices," *Int. J. Antennas Propag.*, vol. 2021, no. 1, p. 2286011, 2021. https://doi.org/10.1155/2021/2286011.

[14] M. Khalily, R. Tafazolli, T. A. Rahman, and M. R. Kamarudin, "Design of phased arrays of series-fed patch antennas with reduced number of the controllers for 28-GHz mm-wave applications," *IEEE Antennas Wireless Propag. Lett.*, vol. 15, pp. 1305–1308, 2015. https://doi.org/10.1109/LAWP.2015.2505781.

[15] H. Zhou, "Phased array for millimeter-wave mobile handset," in *IEEE Antennas and Propagation Society International Symposium (APSURSI)*, 2014, pp. 933–934. https://doi.org/10.1109/APS.2014.6904795.

[16] M. Stanley et al., "A high gain steerable millimeter-wave antenna array for 5G smartphone applications," in *2017 11th European Conference on Antennas and Propagation (EUCAP)*, 2017, pp. 1311–1314. https://doi.org/10.23919/EuCAP.2017.7928542.

[17] J. Helander, K. Zhao, Z. Ying, and D. Sjöberg, "Performance analysis of millimeter-wave phased array antennas in cellular handsets," *IEEE Antennas Wireless Propag. Lett.*, vol. 15, pp. 504–507, 2015. https://doi.org/10.1109/LAWP.2015.2455040.

[18] H. Q. Al-Gburi, M. Algburi, and H. Al-Saedi, "Compact antenna design for RFID and IoT applications," in *2022 2nd International Conference on Computing and Machine Intelligence (ICMI)*, 2022, pp. 1–4. https://doi.org/10.1109/ICMI55296.2022.9873727.

[19] S. F. Abdulkareem, Z. Faydh, and D. H. Al-Nuaimi, "Investigation of dualband fan-shaped microstrip bandpass filter," *TELKOMNIKA (Telecommunication Computing Electronics and Control)*, vol. 19, no. 1, pp. 229–234, 2021. https://doi.org/10.12928/telkomnika.v19i1.16507.

[20] S. K. Ahmed, M. Chandra, and Z. A. A. Hassain, "Reducing the cross-polarization pattern in a dual-polarized antenna using spiral and split ring resonators," *Journal of Engineering and Sustainable Development*, vol. 26, no. 6, pp. 30–38, 2022. https://doi.org/10.31272/jeasd.26.6.4.

[21] Y. S. Mezaal and S. F. Abdulkareem, "New microstrip antenna based on quasi-fractal geometry for recent wireless systems," in *2018 26th Signal Processing and Communications Applications Conference (SIU)*, Izmir, Turkey, 2018, pp. 1–4. https://doi.org/10.1109/SIU.2018.8404727.

[22] Y. S. Mezaal and D. A. Hammood, "New microstrip quasi fractal antennas: Design and simulation results," in *2016 IEEE 36th International Conference on Electronics and Nanotechnology (ELNANO)*, Kyiv, Ukraine, 2016, pp. 75–78. https://doi.org/10.1109/ELNANO.2016.7493014.

[23] C. A. Balanis, *Antenna Theory: Analysis and Design*, 3rd ed. Hoboken, NJ: Wiley, 2005, pp. 523–524, 865–866.

[24] E. Sandi, A. D. Rusmono, A. Diamah, and K. Vinda, "Ultra-wideband microstrip array antenna for 5G millimeter-wave applications," *J. Commun.*, vol. 15, no. 2, pp. 198–204, 2020. https://doi.org/10.12720/jcm.15.2.198-204.